Noise in Brillouin based information storage

OSCAR A. NIEVES,[1] MATTHEW D. ARNOLD,[1] MIKOŁAJ K. SCHMIDT,[2] MICHAEL J. STEEL,[2] AND CHRISTOPHER G. POULTON[1,*]

[1] *School of Mathematical and Physical Sciences, University of Technology Sydney, 15 Broadway, Ultimo NSW 2007, Australia*
[2] *Deparment of Physics and Astronomy, Macquarie University, North Ryde NSW 2109, Australia*
[*]christopher.poulton@uts.edu.au

Abstract: We theoretically and numerically study the efficiency of Brillouin-based opto-acoustic data storage in a photonic waveguide in the presence of thermal noise and laser phase noise. We compare the physics of the noise processes and how they affect different storage techniques, examining both amplitude and phase storage schemes. We investigate the effects of storage time and pulse properties on the quality of the retrieved signal and find that phase storage is less sensitive to thermal noise than amplitude storage.

1. Introduction

Stimulated Brillouin scattering (SBS) is an opto-acoustic process that results from the coherent interaction between two counter-propagating optical fields and an acoustic wave inside an optical waveguide [1–5]. In backward SBS, a pump field at frequency ω_1 is injected at one end of the waveguide, and a counter-propagating field at the Brillouin Stokes frequency $\omega_2 = \omega_1 - \Omega$, where Ω is the Brillouin frequency shift, is injected at the other; the interaction of these two fields creates a strong acoustic wave at frequency Ω. When the Stokes power is comparable in size to the pump power, the pump energy can be completely depleted and some of it transferred to the acoustic field, along with its amplitude and phase information. A recent application of this effect is opto-acoustic memory storage (see Fig. 1): an optical data pulse at the pump frequency interacts with an optical "write" pulse (at the Stokes frequency), creating an acoustic hologram where the original data is temporarily stored [6–8]; an optical "read" pulse at the Stokes frequency can then be used to regenerate the original data pulse. Brillouin-based opto-acoustic information storage has been demonstrated experimentally in fibres [6] as well as more recently in on-chip experiments [7–12], with storage times ranging up to 40 ns [12]. Opto-acoustic storage, however, will inevitably be limited by noise, which exists because of the presence of thermal phonons in the waveguide, as well as being an inherent feature of the lasers used in the data and read/write pulses. At room temperatures, it is known that thermal noise significantly degrades the quality of Brillouin processes [13–18], and it can be expected that it will also place limits on information *retrieval efficiency* in Brillouin storage experiments, measured as the amount of power that can be retrieved from the acoustic field after a certain time. This has been experimentally measured [6,11], however while noise has been observed as a feature of these experiments, it is not yet clear how noise impacts the accuracy of the information retrieval. Furthermore, most studies (except, notably, [10]) have focused on amplitude encoded storage, in which bits of information are stored in individual pulses. Alternatively, phase encoded storage may offer higher storage efficiency and be less sensitive to noise. A quantitative understanding of the impact of noise on the storage of both amplitude and phase information is needed for the further development of practical Brillouin-based storage devices.

In this paper, we apply our previous theoretical [18] and numerical [19] models to the simulation of Brillouin storage in the presence of thermal noise. These studies focused on the
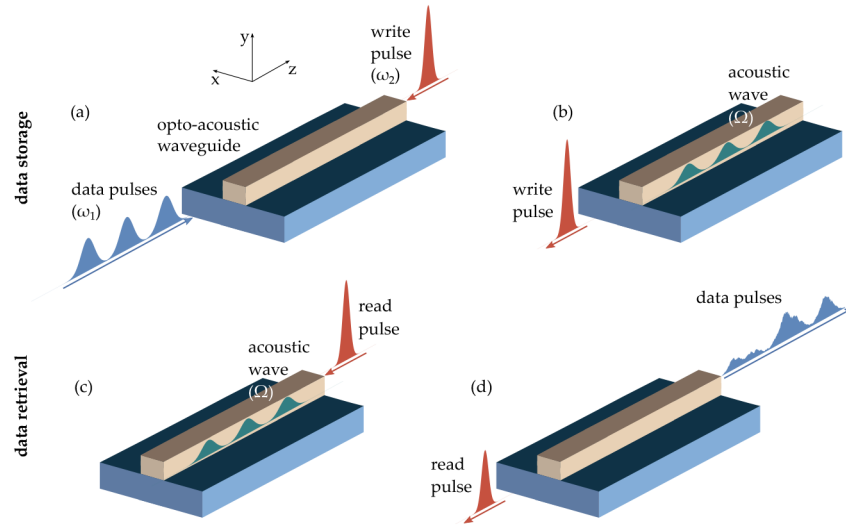
Fig. 1. Illustration of the opto-acoustic storage achieved via SBS, neglecting the effects of noise, and using amplitude shift-keying (amplitude storage). Storage process in (a) and (b): data pulses are depleted by the write-pulse, exciting an acoustic wave inside the waveguide, with some energy gained by the write-pulse. Retrieval process in (c) and (d): a read-pulse interacts with the acoustic wave, both become depleted and the energy is used to regenerate the original sequence of data pulses. The retrieval efficiency is limited by the acoustic lifetime of the phonons.

noise properties of optical pulses in the case of SBS amplification, with the pump containing a lot more power than the input Stokes seed. Here, we investigate the effect of noise on both amplitude and phase storage of information, by using a small pump power and a large Stokes seed power. We quantify the retrieval efficiency and accuracy in the form of the packet error rate (PER) of 8-bit sequences. We find that phase storage offers a significant improvement in the duration with which information can be stored without degradation due to thermal noise. We examine this effect in more detail by computing the effect of thermal noise on the amplitude and phase of a phase-encoded signal, and find that although the variance in amplitude and phase increases at the same rates, the phase information is more robust to noise in accordance with the additive-white-Gaussian-noise (AWGN) model of discrete communication theory.

2. Numerical simulation of noise

2.1. Brillouin coupled mode equations

We consider a waveguide of length L oriented along the z coordinate axis, in which an optical data stream propagates in the positive z direction. The interaction between the two optical fields and the acoustic field can be described by the coupled system [18,19]

$$\frac{\partial a_1}{\partial z} + \frac{1}{v}\frac{\partial a_1}{\partial t} + \frac{1}{2}\alpha a_1 = i\omega_1 Q_1 a_2 b^*, \tag{1}$$

$$\frac{\partial a_2}{\partial z} - \frac{1}{v}\frac{\partial a_2}{\partial t} - \frac{1}{2}\alpha a_2 = i\omega_2 Q_2 a_1 b, \tag{2}$$

$$\frac{\partial b}{\partial z} + \frac{1}{v_a}\frac{\partial b}{\partial t} + \frac{1}{2}\alpha_{\mathrm{ac}} b = i\Omega Q_a a_1^* a_2 + \sqrt{k_B T \alpha_{\mathrm{ac}}} R(z,t), \tag{3}$$

where $a_1(z, t)$ and $a_2(z, t)$ are the envelope fields of the data pulse (pump) and read/write pulse (Stokes) respectively, which correspond to mode fields with frequency/wavenumber ($\omega_{1,2}, k_{1,2}$). $b(z, t)$ is the acoustic envelope field for the mode with frequency/wavenumber (Ω, q). All envelope fields have units of $W^{1/2}$. In these equations the optical group velocity is given by $v > 0$ and the acoustic group velocity is denoted $v_a > 0$. α and α_{ac} are the optical and acoustic loss coefficients respectively (in units of m^{-1}). The coefficients $Q_{1,2,a}$ represent the coupling strength of the SBS interaction, which depend on the optical and acoustic modes of the waveguide [20]; from local conservation of energy, we have $Q_1 = -Q_2^*$ and $Q_a = Q_2^*$ [21]. These parameters are related to the SBS gain parameter g_0 (with units of $m^{-1}W^{-1}$), via the expression $Q_2 = \sqrt{g_0 \Gamma / (4 v_a \omega_2 \Omega)}$, where $\Gamma = v_a \alpha_{ac} = 1/\tau_a$ is the rate of decay of the phonons. In deriving Eq. (1)−(3) we have assumed the phase matching conditions $\Omega = \omega_1 - \omega_2$ and $q = k_1 - k_2$.

The thermal noise is represented by a zero-mean space-time white noise function, with auto-correlation function given by $\langle R(z, t) R(z', t') \rangle = \delta(z - z') \delta(t - t')$. The parameter $k_B T \alpha_{ac}$ is the strength of the thermal noise, which arises from the fluctuation-dissipation theorem [18]. The functions describing the data stream and the read-write pulses are given by $a_{data}(t)$, $a_{read}(t)$ and $a_{write}(t)$, which describe the values of the optical envelopes at $z = 0$ (data) and $z = L$ (read/write). To incorporate phase noise from the lasers used to generate these fields, the envelope fields at the ends of the waveguide are specified by stochastic boundary conditions, namely $a_1(0, t) = a_{data}(t) e^{i\phi_1(t)}$ for the data pulse and $a_2(L, t) = [a_{read}(t) + a_{write}(t)] e^{i\phi_2(t)}$. The random phase terms $\phi_{1,2}$ are statistically uncorrelated Brownian motions described by

$$\phi_j(t) = \sqrt{2\pi \Delta \nu_L} \int_{-\infty}^{t} dW(t), \quad (4)$$

where $dW(t)$ is a standard Wiener increment [22], and $\Delta \nu_L$ is the laser's intrinsic linewidth [19].

In non-storage SBS setups [18,19] the pump has higher input power P_{p0} than the Stokes P_{s0} and thus behaves as an amplifier. However, in the case of Brillouin storage, we require $P_{p0} \ll P_{s0}$ so that the read/write pulse can completely deplete the pump, which contains the data to be stored. Optimum storage requires two conditions on the read/write pulse. First, the read/write pulses must be at least as short in duration as the shortest data pulse. Second, the pulse area for the read/write pulse, defined as [6,23]

$$\Theta_w = \sqrt{\frac{g_0 v}{8 \tau_a}} \int_{-\infty}^{\infty} a_{read/write}(t) dt, \quad (5)$$

must obey the condition $\Theta_w = (m + 1/2)\pi$ where $m = 0, 1, 2, \ldots$. This is because once the data pulse is depleted completely, the transfer of energy reverses and the data pulse is regenerated [23–25]. The dependence of the pulse-area on τ_a may seem deceptive at first, but since g_0 is also dependent on τ_a these two effects cancel out.

The storage efficiency tells us how effective the storage system is, and may be defined as the ratio of the total output data power $|a_{out}(t)|^2$ to the total input data power $|a_{data}(t)|^2$ [10]:

$$\eta_{sto} = \frac{\int_0^{\tau_{data}} \langle |a_{out}(t)|^2 \rangle dt}{\int_0^{\tau_{data}} \langle |a_{data}(t)|^2 \rangle dt}, \quad (6)$$

where $\langle X(t) \rangle = \frac{1}{N} \sum_{n=1}^{N} X_n(t)$ is the ensemble average of a function $X(t)$ over N independent runs, and τ_{data} is the duration of the data train. Because the acoustic wave decays in time at a rate $1/\tau_a$, η_{sto} decreases with longer storage times, reducing the efficiency in addition to the effects of noise. We define the storage time τ_{sto} as the temporal delay between the write and read pulses.

2.2. Solution to the coupled mode equations

We numerically solve Eq. (1)−(3) following the numerical method described in [19]. In brief, we note that the propagation distance of the acoustic wave over the time-scale of the SBS interaction

is very small [13]. We therefore apply the limit $\partial_z b \to 0$ in Eq. (3), and solve the equation in time via the Green function method [18]. The thermal noise function is simulated starting at thermal equilibrium at $t = 0$, by drawing random numbers from a steady-state probability distribution corresponding to an Ornstein-Uhlenbeck process [19,26]. We then substitute the formal solution $b(z, t)$ into Eq. (1) and (2), and integrate the two equations using a two-step iteractive method: first, the optical fields are translated in space by a distance $\Delta z = v\Delta t$ while the acoustic field remains stationary [19]. Then, the optical fields at each point in space z are updated by integrating the equations in time with an Euler-Mayurama scheme [27]. This two-step process is iterated over multiple time steps to simulate the dynamics of the input pulses.

For our simulations we use the parameters summarized in Table 1. We assume a high gain chalcogenide waveguide, of the type used in previous SBS experiments [28]. We store individual 8-bit packets one at a time, consisting of all 256 possible unique 8-bit sequences. Each packet corresponds to 8 individual pulses in the amplitude storage case, and 4 phases in the phase storage case, as shown in Fig. 2.

Table 1. Parameters used in this study. Physical parameters correspond to a chalcogenide waveguide [28].

Parameter	Value	Parameter	Value
Waveguide length L	30 cm	Peak read/write power	0.5−10.5 W
Waveguide temperature T	300 K	Data packets	256
Refractive index n	2.44	Data stream duration τ_{data}	2.44 ns
Acoustic velocity v_a	2500 m/s	Bit duration τ_{bit}	300 ps
Acoustic lifetime τ_a	10.2 ns	Data pulse width τ_1	150 ps
Brillouin shift $\Omega/2\pi$	7.8 GHz	Read pulse width τ_2	100 ps
Brillouin gain parameter g_0	411 m^{-1}W^{-1}	Grid size (space) N_z	800
Optical wavelength λ	1550 nm	Grid size (time) N_t	2797
Laser linewidth $\Delta\nu_L$	100 kHz	Step-size Δz	375 μm
Peak data power	10 mW	Step-size Δt	3.05 ps
Optical loss α	0.1 dB/cm		

It should be noted that the model used here (Eq. (1)−(3)) makes the assumption of the slowly-varying envelope approximation (SVEA) and rotating-wave approximation (RWA) [18,21]. Because the acoustic frequencies used in SBS experiments are typically in the range of a few GHz [1,29], the optical pulses simulated must be longer than a few hundred picoseconds in duration so that these approximations remain valid [30]. Therefore, we limit our simulations to pulses no shorter than 100 ps, for both for the data and read/write cases. We have chosen to focus on the storage of 8-bit sequences because they can fit inside a 30 cm chalcogenide waveguide without being too short to violate the SVEA and RWA for a 7.8 GHz Brillouin frequency shift, since the acoustic pulses generated from 300 ps optical bits are approximately 3.7 cm in length.

2.3. Data encoding

The two storage schemes used in this paper — amplitude and phase storage — are summarized in Fig. 2. Each bit is defined as having a duration τ_{bit}. For amplitude storage, we encode ones into Gaussian pulses of the same peak power P_{p0}, while zeros are represented by gaps of duration τ_{bit}. For phase storage, we use the same scheme as in quadrature phase-shift keying (QPSK) with gray coding [31], where bit pairs are assigned a unique phase, namely 11 = 45°, 01 = 135°, 00 = 225° and 10 = 315°. For a given input information packet, we quantify the retrieval accuracy in both storage schemes via the packet error rate (PER). This is similar to the bit error rate (BER) of a binary stream, except that we count correct 8-bit packets as opposed to counting individual
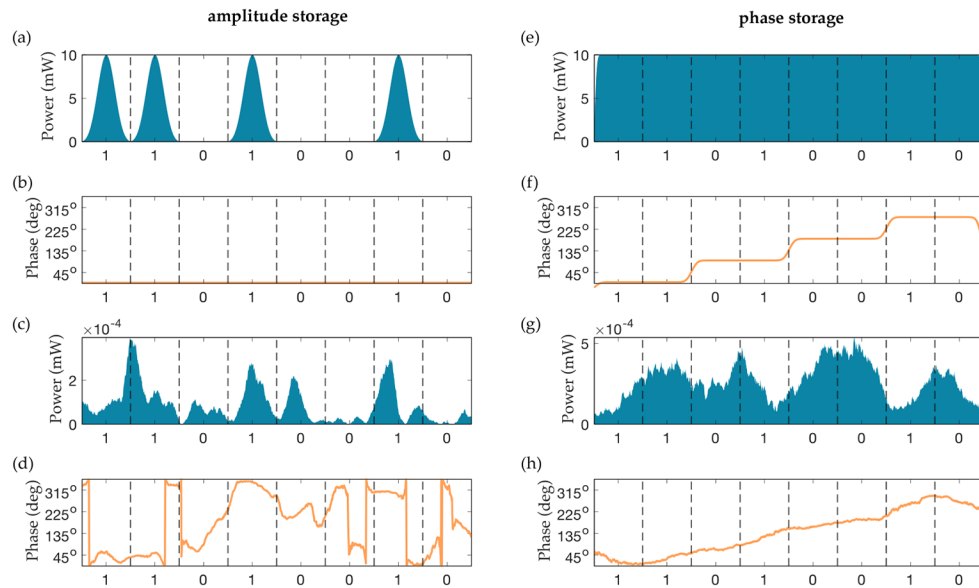
Fig. 2. Illustration of how the 8-bit sequence $\mathbf{x} = 11010010$ is encoded in the numerical simulation. Amplitude storage: (a)−(b) input power and phase, (c)−(d) output power and phase after some storage time. Phase storage: (e)−(f) input power and phase, (g)−(h) output power and phase after some storage time. Here we use thermal noise at $T = 300$ K.

correct bits. Therefore, the PER is the ratio of correctly retrieved packets with respect to the input data, and has a value $0 \leq \text{PER} \leq 1$.

In the amplitude storage case, we encode bits=1 into Gaussian pulses of full-width at half-maximum (FWHM) τ_1, while bits=0 are represented by gaps of duration τ_{bit} in the data sequence. By default, we choose all pulses to have a phase of $0°$. In the retrieval stage, the output data power $|a_{\text{out}}(t)|^2$ is separated into equal intervals of length τ_{bit}. We use a dynamic threshold technique: initially, a threshold power P_{thresh} is set. Then, we record the output power at the center of the bit
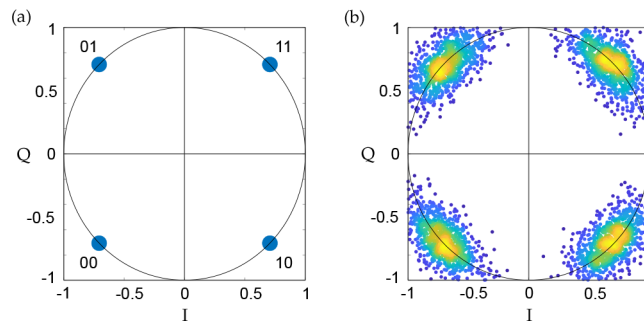

Fig. 3. Constellation diagrams used in phase storage. These plots are done on the complex plane, where the modulus of each point corresponds to the normalized power of the signal, and the argument corresponds to the phase of the signal. (a) ideal system: each point lies at exactly $45°$ from the horizontal line in either direction, and on the circle of radius 1. (b) Effect of noise in the detected signal: amplitude noise shifts the points in the radial direction, while phase noise shifts the points in the angular direction, and the color scheme shows the regions of higher or lower density of points.

period, and a single bit is read as 0 if $|a_{\text{out}}^{(n)}(t)|^2 < P_{\text{thresh}}$ and as 1 if $|a_{\text{out}}^{(n)}(t)|^2 \geq P_{\text{thresh}}$ [32], for all 256 data packets. This process is repeated for different values of P_{thresh} until the total PER has been minimized.

In the phase storage case, we encode bit-pairs into 4 different phases, as shown in Fig. 3(a), as part of an analytic smooth rectangular pulse (ASR) [33] with FWHM τ_{data}. We then apply a Gaussian filter to remove non-physical discontinuities; to emulate the effect of the modulators used in SBS experiments we have chosen a filter width of 5 GHz, resulting in a smooth phase transition between the bit-pairs (see Fig. 2(f)). In the retrieval stage, $|a_{\text{out}}(t)|^2$ is separated into equal intervals of length $2\tau_{\text{bit}}$. We extract the phase from the amplified output signal as $\phi_{\text{out}}(t) = \tan^{-1}\left(\text{Im}\left[a_{\text{out}}(t)\right]/\text{Re}\left[a_{\text{out}}(t)\right]\right)$. We assume ideal detector conditions and record the phase at the center of the $2\tau_{\text{bit}}$ period, such that if $0° < \phi_{\text{out}}(t) < 90°$, we read the output bit-pair as 11, if $90° < \phi_{\text{out}}(t) < 180°$ we read the bit-pair as 01 and so on. Additionally, we use another measure of signal integrity based on the constellation diagram data: let $z_{\text{out}}^{(m)}$ represent a single point on the constellation diagram corresponding to the mth bit-pair in the binary sequence (such as 00), with magnitude $\left|z_{\text{out}}^{(m)}\right|$ and phase ϕ_z^{m}. The variances in each can be found via

$$\text{Var}\left[\left|z_{\text{out}}^{(m)}\right|\right] = \left\langle\left|z_{\text{out}}^{(m)}\right|^2\right\rangle - \left\langle\left|z_{\text{out}}^{(m)}\right|\right\rangle^2, \quad \text{Var}\left[\phi_{\text{out}}^{(m)}\right] = \left\langle\left(\phi_{\text{out}}^{(m)}\right)^2\right\rangle - \left\langle\phi_{\text{out}}^{(m)}\right\rangle^2. \tag{7}$$

3. Results and discussion

3.1. Effect of thermal noise

We investigate the effect of varying the read/write pulse peak power between 0.5−10.5 W, while maintaining a read/write pulse width of 100 ps. We include thermal noise into the waveguide at 300 K, but neglect the input laser phase noise by setting the laser linewidth $\Delta\nu_L$ to zero. In the amplitude storage case, we use Gaussian data pulses with 10 mW peak power and pulse width 150 ps, while in the phase storage case we use a rectangular pulse of duration 2.44 ns, and phase intervals of duration 600 ps. Each bit of optical information is 300 ps in length for both amplitude and phase storage. The results of the simulations are shown in Fig. 4. First, we observe in Fig. 4(a) and (b) that the storage efficiency in both storage schemes is higher as we increase the peak write pulse power, as the pulse area is lower than the optimum value given by Eq. (5). Second, we see in Fig. 4(c) and (d) that lower peak write powers lead to increased PER, thus reducing the maximum storage time achievable in both encoding schemes. This occurs because at lower peak read/write powers — which also corresponds to the lower storage efficiency regime — the coherent output data field is less distinguishable from the amplified spontaneous noise arising from the interaction between the read/write pulse and the thermal background fluctuations in the waveguide [18,19]. Consequently, this increases the probability of retrieving the wrong data sequence at the waveguide output ($z = L$).

Similarly, we see an increase in PER in both AS and PS schemes with increasing τ_{sto}, as shown in Fig. 4(c) and (d). This occurs because in the time between the write and read-process, the acoustic wave containing the stored information decays at a rate $1/\tau_a$. As τ_{sto} increases, the acoustic wave gets closer to the background thermal noise, increasing the fluctuations in the retrieved data field during the read-process. This effect is more clearly illustrated in Fig. 5, where the constellation points spread out in both radial and angular directions, indicating an increase in both amplitude and phase noise in the retrieved data field. In Fig. 6 we see that the rate of increase in the variance of the phase and amplitude of each encoding scheme is the same for the first 40 nanoseconds. However, in Fig. 4(f) we see that the PER in the phase storage case begins to increase at longer τ_{sto} compared to the amplitude storage case, suggesting that phase-encoded data is more robust to thermal noise and hence allows for longer storage times. This occurs because the phase variations are primarily constrained to a single quadrant on the constellation
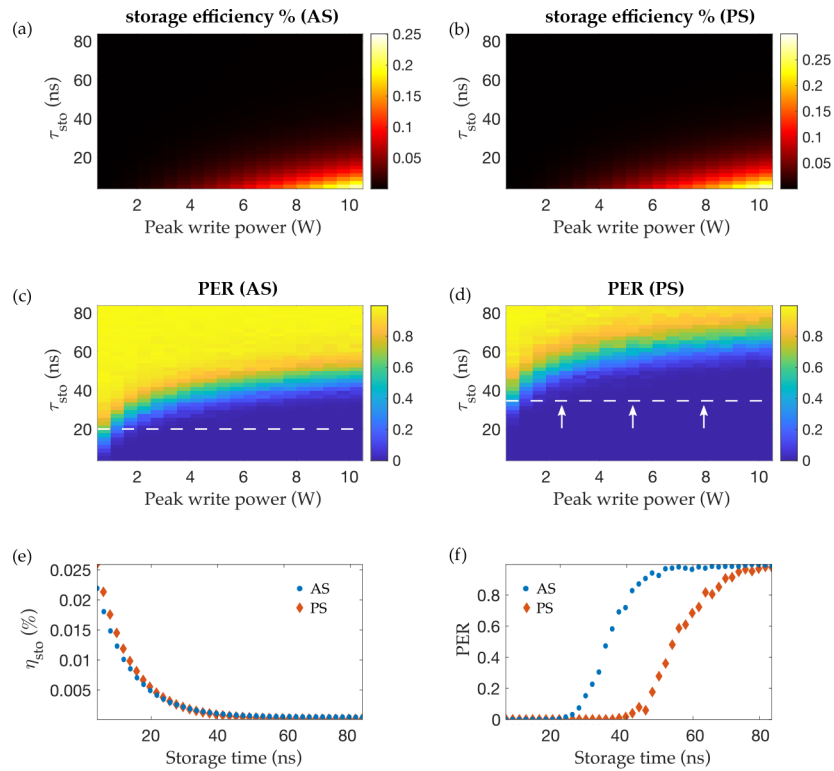
Fig. 4. Simulations of Brillouin storage with thermal noise only, for varying read/write pulse peak power and different storage times in amplitude storage and phase storage. Panels (a) and (b) show the storage efficiency of the two schemes, (c) and (d) the packet error rates, (e) and (f) illustrate the storage efficiency and PER at 3 W peak write power. The dashed horizontal line in (c) and (d) indicates the τ_{sto} at which data packet errors begin to occur, and the arrows in (d) show that this threshold is pushed further back in time.

plots (as shown in Fig. 5), whereas the amplitude variations reach the noise floor more rapidly. Consequently, the probability of detecting the wrong bit of information in the amplitude is higher compared to the phase. This is the same observation that would be expected from the additive white Gaussian noise (AWGN) model in discrete communication theory, where the probability of bit error for phase-shift-keying (PSK) is lower than for amplitude-shift-keying (ASK) [34,35]. In addition, phase encoding can transfer more bits per symbol, which allows for the use of longer optical pulses without loss of data capacity.

3.2. Effect of laser phase noise

We now investigate the effect of adding input laser phase noise, at a linewidth of 100 kHz, with the same pulse and thermal noise parameters as before. We generate the phase noise in the data pulses and read/write pulses independently so they are statistically uncorrelated, but have the same mean and variance properties. Figure 7 shows the results for storage efficiency and PER for both encoding schemes. The plots in Fig. 7(a)−(d) look very similar to Fig. 4(a)−(d), indicating that laser phase noise does not have a significant impact on the storage efficiency or PER. This is consistent with previous work on SBS noise in short pulses [19], where it was found that laser phase noise only has a significant impact on the SBS process when the laser coherence time ($\tau_{coh} = 1/\pi\Delta\nu_L$) is comparable in magnitude to the SBS interaction time. Next, the constellation
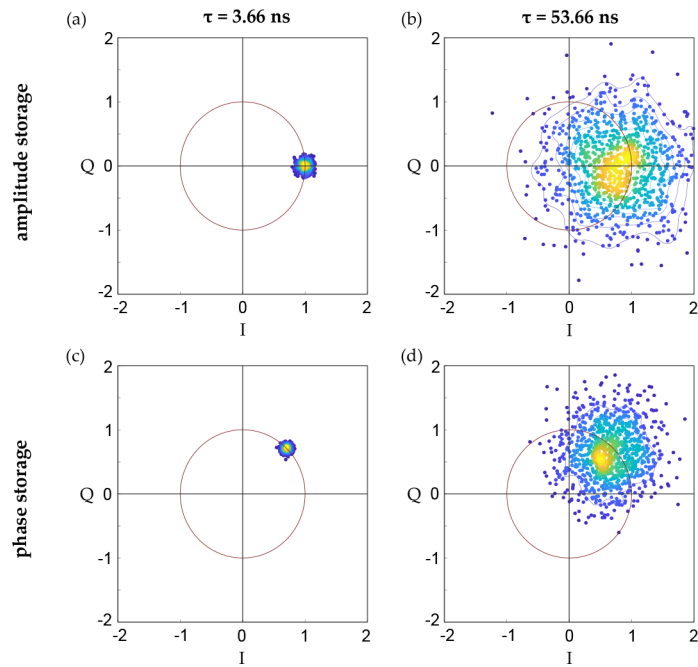
Fig. 5. Constellation diagrams for the thermal noise only case, at 3 W peak write power. (a) and (b) show the amplitude storage plots at two storage times (3.66 ns is the minimum storage time achievable in this configuration) for a binary bit 1, while (c) and (d) show the phase storage plots for a binary bit pair 11.
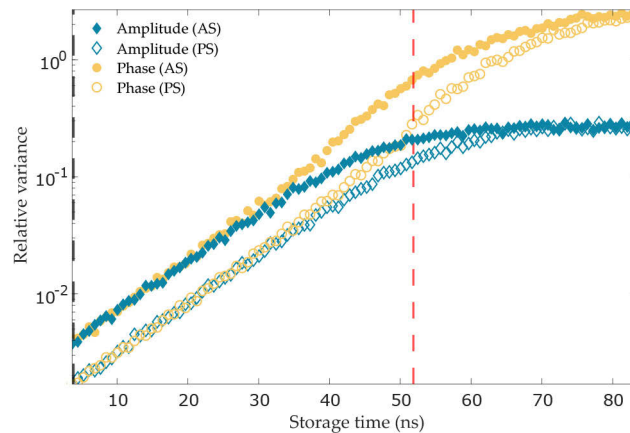

Fig. 6. Relative variance in the amplitude and phase of the constellation data in Fig. 5 as a function of storage time. The dashed lines mark the storage times corresponding to the constellation diagrams in Fig. 5.

diagram results in Fig. 8 reveal that the input laser phase noise broadens the variance in the phase of the retrieved data field, making the distribution of constellation points slightly more elliptical compared to the thermal noise only case. This is also shown in Fig. 9, where the rates of increase for the amplitude and phase variances still remain approximately the same for the first 40 nanoseconds of storage time. This occurs because at this regime of powers for the data pulses, the SBS process acts as a linear amplifier, hence the total noise in the retrieved data is a linear combination of the waveguide thermal noise and the laser phase noise from the inputs.
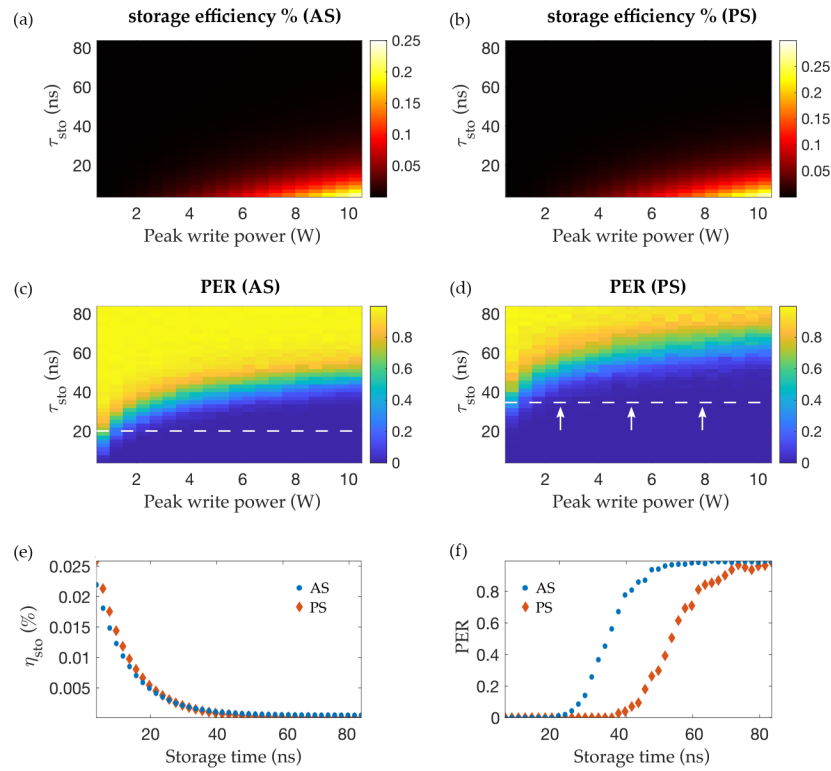

Fig. 7. Simulations of Brillouin storage with both thermal and laser phase noise, for varying read/write pulse peak power and different storage times in amplitude storage and phase storage. Panels (a) and (b) show the storage efficiency of the two schemes, (c) and (d) the packet error rates, (e) and (f) illustrate the storage efficiency and PER at 3 W peak write power. The dashed horizontal line in (c) and (d) indicates the τ_{sto} at which data packet errors begin to occur, and the arrows in (d) show that this threshold is pushed further back in time.
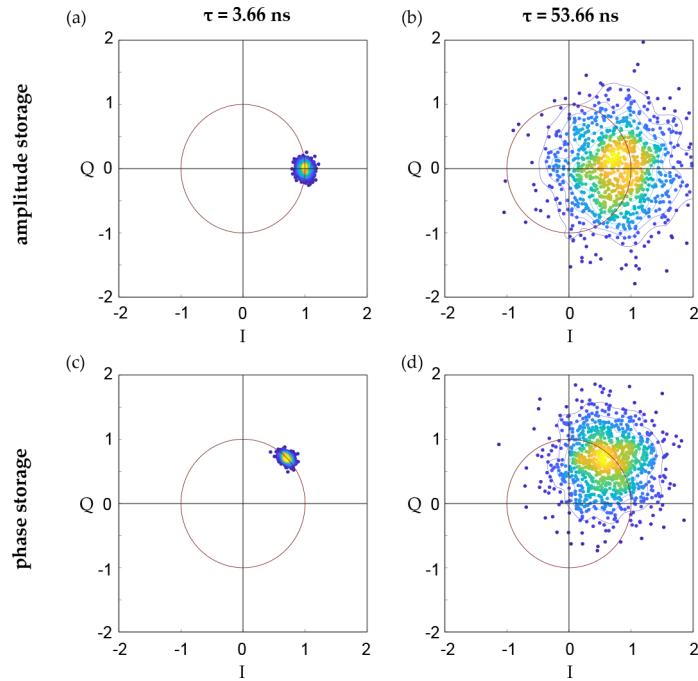
Fig. 8. Constellation diagrams for the thermal noise and laser phase noise case, at 3 W peak write power. (a) and (b) show the amplitude storage plots at two storage times (3.66 ns is the minimum storage time achievable in this configuration) for a binary bit 1, while (c) and (d) show the phase storage plots for a binary bit pair 11.
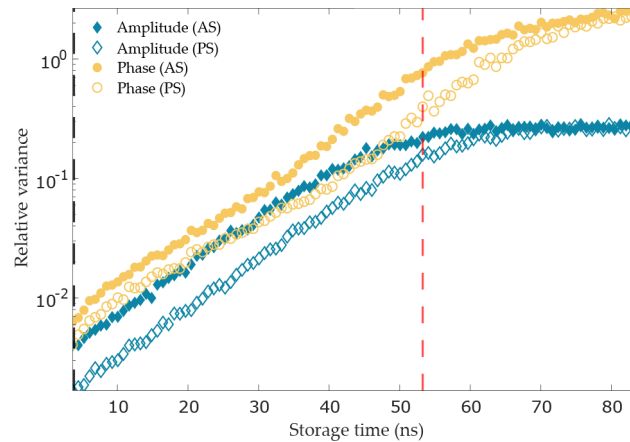

Fig. 9. Relative variance in the amplitude and phase of the constellation data in Fig. 8 as a function of storage time. The dashed lines mark the storage times corresponding to the constellation diagrams in Fig. 8.

4. Conclusion

We have numerically simulated the Brillouin storage of different data packets with thermal and laser noise, using amplitude storage and phase storage techniques in a photonic waveguide. Through these computer simulations, we have shown that phase encoded storage allows for longer storage times than amplitude encoded storage. This is because phase encoding is more robust to noise than amplitude encoding, in accordance with the additive-white-Gaussian-noise model of discrete communications theory [34]. It is therefore possible to increase Brillouin storage time by encoding information into the phase of the data field, without having to change the waveguide or laser properties. Furthermore, because phase storage techniques can encode more bits per symbol than amplitude storage [31,34], one can use longer optical pulses without loss of data capacity.

Disclosures. The authors declare no conflicts of interest.

Data availability. Data underlying the results presented in this paper are not publicly available at this time but may be obtained from the authors upon reasonable request.

References

1. B. J. Eggleton, C. G. Poulton, P. T. Rakich, M. J. Steel, and G. Bahl, "Brillouin integrated photonics," Nat. Photonics **13**(10), 664–677 (2019).
2. A. Kobyakov, M. Sauer, and D. Chowdhury, "Stimulated Brillouin scattering in optical fibers," Adv. Opt. Photonics **2**(1), 1–59 (2010).
3. R. Pant, D. Marpaung, I. V. Kabakova, B. Morrison, C. G. Poulton, and B. J. Eggleton, "On-chip stimulated Brillouin scattering for microwave signal processing and generation," Laser Photonics Rev. **8**(5), 653–666 (2014).
4. R. W. Boyd, *Nonlinear optics* (Elsevier, 2003).
5. L. Brillouin, "Diffusion de la lumière et des rayons X par un corps transparent homogène," Ann. Phys. **9**(17), 88–122 (1922).
6. Z. Zhu, D. J. Gauthier, and R. W. Boyd, "Stored light in an optical fiber via stimulated Brillouin scattering," Science **318**(5857), 1748–1750 (2007).
7. V. Kalosha, W. Li, F. Wang, L. Chen, and X. Bao, "Frequency-shifted light storage via stimulated Brillouin scattering in optical fibers," Opt. Lett. **33**(23), 2848–2850 (2008).
8. M. Merklein, B. Stiller, and B. J. Eggleton, "Brillouin-based light storage and delay techniques," J. Opt. **20**(8), 083003 (2018).
9. C.-H. Dong, Z. Shen, C.-L. Zou, Y.-L. Zhang, W. Fu, and G.-C. Guo, "Brillouin-scattering-induced transparency and non-reciprocal light storage," Nat. Commun. **6**(1), 6193–6196 (2015).
10. M. Merklein, B. Stiller, K. Vu, S. J. Madden, and B. J. Eggleton, "A chip-integrated coherent photonic-phononic memory," Nat. Commun. **8**(1), 574–577 (2017).
11. M. Merklein, B. Stiller, K. Vu, P. Ma, S. J. Madden, and B. J. Eggleton, "On-chip broadband nonreciprocal light storage," Nanophotonics **10**(1), 75–82 (2020).
12. B. Stiller, M. Merklein, C. Wolff, K. Vu, P. Ma, S. J. Madden, and B. J. Eggleton, "Coherently refreshing hypersonic phonons for light storage," Optica **7**(5), 492–497 (2020).
13. R. W. Boyd, K. Rzazewski, and P. Narum, "Noise initiation of stimulated Brillouin scattering," Phys. Rev. A **42**(9), 5514–5521 (1990).
14. A. L. Gaeta and R. W. Boyd, "Stochastic dynamics of stimulated Brillouin scattering in an optical fiber," Phys. Rev. A **44**(5), 3205–3209 (1991).
15. M. Ferreira, J. Rocha, and J. Pinto, "Analysis of the gain and noise characteristics of fiber Brillouin amplifiers," Opt. Quantum Electron. **26**(1), 35–44 (1994).
16. P. Kharel, R. Behunin, W. Renninger, and P. Rakich, "Noise and dynamics in forward Brillouin interactions," Phys. Rev. A **93**(6), 063806 (2016).
17. R. O. Behunin, N. T. Otterstrom, P. T. Rakich, S. Gundavarapu, and D. J. Blumenthal, "Fundamental noise dynamics in cascaded-order Brillouin lasers," Phys. Rev. A **98**(2), 023832 (2018).
18. O. A. Nieves, M. D. Arnold, M. Steel, M. K. Schmidt, and C. G. Poulton, "Noise and pulse dynamics in backward stimulated Brillouin scattering," Opt. Express **29**(3), 3132–3146 (2021).

19. O. A. Nieves, M. D. Arnold, M. J. Steel, M. K. Schmidt, and C. G. Poulton, "Numerical simulation of noise in pulsed Brillouin scattering," J. Opt. Soc. Am. B **38**(8), 2343–2352 (2021).

20. B. C. Sturmberg, K. B. Dossou, M. J. Smith, B. Morrison, C. G. Poulton, and M. J. Steel, "Finite element analysis of stimulated Brillouin scattering in integrated photonic waveguides," J. Lightwave Technol. **37**(15), 3791–3804 (2019).

21. C. Wolff, M. J. Steel, B. J. Eggleton, and C. G. Poulton, "Stimulated Brillouin scattering in integrated photonic waveguides: Forces, scattering mechanisms, and coupled-mode analysis," Phys. Rev. A **92**(1), 013836 (2015).

22. W. Horsthemke, "Noise induced transitions," in *Non-equilibrium dynamics in chemical systems*, (Springer, 1984), pp. 44–49.

23. M. Dong and H. G. Winful, "Area dependence of chirped-pulse stimulated Brillouin scattering: implications for stored light and dynamic gratings," J. Opt. Soc. Am. B **32**(12), 2514–2519 (2015).

24. H. G. Winful, "Chirped Brillouin dynamic gratings for storing and compressing light," Opt. Express **21**(8), 10039–10047 (2013).

25. L. Allen and J. H. Eberly, *Optical resonance and two-level atoms*, vol. 28 (John Wiley & Sons., 1975).

26. G. E. Uhlenbeck and L. S. Ornstein, "On the theory of the Brownian motion," Phys. Rev. **36**(5), 823–841 (1930).

27. P. Kloeden and E. Platen, *Numerical Solution of Stochastic Differential Equations* (Springer-Verlag, Berlin Heidelberg, 1992), 1st ed.

28. Y. Xie, A. Choudhary, Y. Liu, D. Marpaung, K. Vu, P. Ma, D.-Y. Choi, S. Madden, and B. J. Eggleton, "System-level performance of chip-based Brillouin microwave photonic bandpass filters," J. Lightwave Technol. **37**(20), 5246–5258 (2019).

29. C. Wolff, M. Smith, B. Stiller, and C. Poulton, "Brillouin scattering—theory and experiment: tutorial," J. Opt. Soc. Am. B **38**(4), 1243–1269 (2021).

30. J. Piotrowski, M. K. Schmidt, B. Stiller, C. G. Poulton, and M. J. Steel, "Picosecond acoustic dynamics in stimulated Brillouin scattering," Opt. Lett. **46**(12), 2972–2975 (2021).

31. S. Faruque, *Radio frequency modulation made easy* (Springer, 2017), pp. 69–83.

32. D. Walsh, D. Moodie, I. Mauchline, S. Conner, W. Johnstone, and B. Culshaw, "Practical bit error rate measurements on fibre optic communications links in student teaching laboratories," in *9th International Conference on Education and Training in Optics and Photonics (ETOP)*, Marseille, France, Paper ETOP021, (2005).

33. E. Granot, "Propagation of chirped rectangular pulses in dispersive media: analytical analysis," Opt. Lett. **44**(19), 4745–4748 (2019).

34. D. R. Smith, *Digital transmission systems* (Springer science & business media, 2012), pp. 370–381.

35. D. Bala, "Analysis the probability of bit error performance on different digital modulation techniques over AWGN channel using MATLAB," J. Electr. Eng. Electron. Control. Comput. Sci. **7**, 9–18 (2021).